OXFORD

Social Cognitive and Affective Neuroscience, 2020, 1034–1045

doi: 10.1093/scan/nsaa050
Advance Access Publication Date: 17 April 2020
Original Manuscript

Health Neuroscience Special Issue

Affective brain patterns as multivariate neural correlates of cardiovascular disease risk

Peter J. Gianaros,[1,2] Thomas E. Kraynak,[1,2] Dora C.-H. Kuan,[1] James J. Gross,[3] Kateri McRae,[4] Ahmad R. Hariri,[5] Stephen B. Manuck,[2] Javier Rasero,[6] and Timothy D. Verstynen[2,6]

[1]Department of Psychology, University of Pittsburgh, Pittsburgh, PA 15260, USA, [2]Center for the Neural Basis of Cognition, University of Pittsburgh and Carnegie Mellon University, Pittsburgh, PA 15213, USA, [3]Department of Psychology, Stanford University, Stanford, CA, 94305, USA, [4]Department of Psychology, University of Denver, Denver, CO, 80208, USA, [5]Department of Psychology and Neuroscience, Duke University, Durham, NC, 27708, USA, and [6]Department of Psychology, Carnegie Mellon University, Pittsburgh, PA 15213, USA

Correspondence should be addressed to Peter J. Gianaros, Department of Psychology, 3131 Sennott Square, 210 S. Bouquet St., Pittsburgh, PA 15260-9150, USA. E-mail: gianaros@pitt.edu.

Abstract

This study tested whether brain activity patterns evoked by affective stimuli relate to individual differences in an indicator of pre-clinical atherosclerosis: carotid artery intima-media thickness (CA-IMT). Adults (aged 30–54 years) completed functional magnetic resonance imaging (fMRI) tasks that involved viewing three sets of affective stimuli. Two sets included facial expressions of emotion, and one set included neutral and unpleasant images from the International Affective Picture System (IAPS). Cross-validated, multivariate and machine learning models showed that individual differences in CA-IMT were partially predicted by brain activity patterns evoked by unpleasant IAPS images, even after accounting for age, sex and known cardiovascular disease risk factors. CA-IMT was also predicted by brain activity patterns evoked by angry and fearful faces from one of the two stimulus sets of facial expressions, but this predictive association did not persist after accounting for known cardiovascular risk factors. The reliability (internal consistency) of brain activity patterns evoked by affective stimuli may have constrained their prediction of CA-IMT. Distributed brain activity patterns could comprise affective neural correlates of pre-clinical atherosclerosis; however, the interpretation of such correlates may depend on their psychometric properties, as well as the influence of other cardiovascular risk factors and specific affective cues.

Key words: affect; cardiovascular disease risk; emotion; fMRI; machine learning

Introduction

Is there a brain phenotype—*a neural pattern expressed reliably by individuals*—that relates to risk for atherosclerotic cardiovascular disease (CVD)? Answering this question may not only add to a brain-based and mechanistic understanding of CVD, but may also inform approaches to predict and reduce vulnerability to a leading cause of population morbidity and mortality (Gianaros and Jennings, 2018; Kraynak *et al.*, 2018a). Existing evidence suggests that CVD risk relates to individual differences in the functionality of cortical and limbic brain systems that encode, process and orchestrate responses to affective cues and contexts (Kraynak *et al.*, 2018a). Through their interplay with brainstem

Received: 28 August 2019; **Revised:** 18 March 2020; **Accepted:** 6 April 2020

cell groups, these cortical and limbic systems are specifically postulated to link affective information processing to downstream control over autonomic, immune and neuroendocrine parameters of peripheral physiology that may be pathogenic to the heart and blood vessels (Kraynak et al., 2018a). Accordingly, quantifying reliable individual differences in the functionality of brain systems for affective processing may help to identify novel neural correlates of CVD risk. Such affective neural correlates could plausibly complement the use of conventional risk factors in the prediction of CVD. They may also help to provide a brain-based account of epidemiological associations between CVD and peripheral physiological and behavioral correlates of mood and emotion (e.g. Rozanski et al., 1999; Krantz and McCeney, 2002; Suls and Bunde, 2005; DeSteno et al., 2013; Davidson et al., 2018).

At present, several autonomic, immune and neuroendocrine correlates of CVD risk have been associated with the functionality of a particular brain system—the amygdala (for reviews, see Muscatell and Eisenberger, 2012; Thayer et al., 2012; Gianaros and Wager, 2015; Ruiz Vargas et al., 2016; Ginty et al., 2017; Kraynak et al., 2018b). Moreover, individual differences in amygdala function have been associated with clinical cardiovascular endpoints, cardiometabolic outcomes that are conducive to atherosclerotic CVD and even surrogate markers of pre-clinical atherosclerosis that are all presaged by autonomic, immune and neuroendocrine dysregulation. Elevated resting metabolic activity of the amygdala, for example, confers risk for cardiovascular events (Tawakol et al., 2017), incident diabetes (Osborne et al., 2019), the progression of visceral adiposity (Ishai et al., 2019) and non-calcified coronary plaque (Goyal et al., 2018). The latter findings build on earlier cross-sectional evidence that pre-clinical atherosclerosis in the carotid arteries associates with elevated metabolic activity in the medial temporal lobe (Sojkova et al., 2010) and—more specifically—with amygdala reactivity to facial expressions of fear and anger (Gianaros et al., 2008). Elevated amygdala activity at rest or evoked by affective cues may thus comprise a neural correlate of CVD risk.

Not all findings, however, support the latter possibility. Hence, the severity of pre-clinical atherosclerosis was not statistically associated with extracted and averaged levels of amygdala reactivity to unpleasant affective scenes (Gianaros et al., 2014). Furthermore, no statistical associations were observed between conventional indicators of CVD risk (e.g. Framingham risk scores, metabolic syndrome) and stressor-evoked activity in cortical and limbic brain systems, including the amygdala (Lederbogen et al., 2018). Consequently, a still open question is whether CVD risk relates to a reproducible neural correlate that encompasses amygdala activity or activity patterns distributed across other brain systems for affective processes that are likewise implicated in CVD risk, such as the cingulate cortex, medial pre-frontal cortex, insula and cell groups of the brainstem (Oppenheimer and Cechetto, 2016; Gianaros and Jennings, 2018; Kraynak et al., 2018a).

In the latter regard, a limitation to most prior studies of the neural correlates of CVD risk is that they have included small samples that constrain attempts to cross-validate candidate brain phenotypes that are reliably expressed by individuals. This issue is especially important insofar as many conventional and ostensibly affective neuroimaging tasks may not reliably index trait-like individual differences in stimulus-evoked brain activity (Nord et al., 2017; Infantolino et al., 2018; Elliott et al., 2020). As a result, brain metrics derived from such tasks in the context of small sample sizes may exhibit variable or unreliable relationships with other individual difference measures, such as CVD risk markers. Lastly, neuroimaging studies of CVD risk often use mass-univariate or potentially biased region of interest (ROI) quantitative methods that further engender issues with (i) multiple statistical testing, (ii) reproducibility and (iii) accurately identifying whole-brain, distributed (multivariate) and generalizable neural patterns that predict cardiovascular risk variables—beyond localized patterns from just a single brain region (e.g. the amygdala) (Woo et al., 2017).

Accordingly, the present study applied whole-brain, multivariate, machine learning and cross-validation methods to test whether individual differences in a vascular indicator of pre-clinical atherosclerosis and CVD risk (carotid artery intima-media thickness; CA-IMT) are reliably predicted by distributed brain activity patterns assessed by fMRI during three affective information processing tasks. As a pre-clinical marker of CVD risk, CA-IMT increases from a progressive thickening of the intimal and medial layers of the carotid arterial wall (Stein et al., 2008), and it has been widely used to measure the atherosclerotic disease process (Oygarden, 2017; Wendell et al., 2017). CA-IMT associates with pathological and histologic measures of atherosclerosis in autopsy studies (Pignoli et al., 1986; Wong et al., 1993), and it has been shown to predict future CVD events (Peters et al., 2012; Baber et al., 2015; Polak et al., 2017). Two of the three affective fMRI tasks were standard matching-to-sample tasks, in which participants matched human faces depicting various emotions. The final task was an emotion processing and responding task, in which participants viewed neutral and unpleasant images from the International Affective Picture System (IAPS) (Lang et al., 2008) and provided subjective ratings of experienced negative affect. Using three affective fMRI tasks enabled tests of whether any observed predictive associations between brain activity and CA-IMT would generalize across a broader range of affective cues than used previously (Gianaros et al., 2008). And in contrast to prior studies that relied on mass-univariate or ROI-based approaches to identify affective neural correlates of CVD risk, the present study used multivariate and whole-brain analysis methods that combined predictor dimensionality reduction, penalized linear regression and cross-validation as per recent approaches and recommendations for predictive and pattern-based modeling (e.g. Eisenbarth et al., 2016; Woo et al., 2017; Gianaros et al., 2017b; Poldrack et al., 2019; Scheinost et al., 2019). Specifically, patterns of brain activity that were evoked by the affective tasks served as multivariate predictor variables, with CA-IMT serving as the outcome variable. Using nested cross-validation, the multivariate neural predictors of CA-IMT were tested for generalizability among study participants whose data were not used for predictive model building and pattern identification. Secondary analyses tested the (i) specific contribution of the amygdala in explaining variance in CA-IMT—owing to its prominence in past literature—(ii) influences of age, sex and other known cardiovascular risk factors; and (iii) psychometric properties of brain activity changes evoked by the affective tasks.

Materials and methods

Participants

Data reported herein were derived from baseline (cross-sectional) assessments of participants from two studies: the Adult Health and Behavior project—Phase 2— (AHAB-2) and the Pittsburgh Imaging Project (PIP). Both AHAB-2 ($N = 490$) and PIP ($N = 331$) are registries of behavioral, biological and neural correlates of CVD risk among otherwise healthy community-dwelling adults (aged 30–54 years). Across both cohorts, there

was an approximate balance of men and women (AHAB-2: 53% women; PIP: 50% women in the full study samples). All participants provided informed consent. The University of Pittsburgh Human Research Protection Office granted approval for AHAB-2 (Protocol ID: 07040037) and PIP (07110287), as well as their aggregation to create a common data registry (19030174). The Supplementary material provides study details.

Overview of study protocols

AHAB-2 and PIP entailed similar medical interviews, as well as multiple visits to assess sociodemographic factors, pre-clinical atherosclerosis (see below) and CVD risk. The latter included seated resting BP measured over multiple visits, waist circumference and fasting glucose; high-density lipoprotein cholesterol (HDL); total cholesterol; and triglycerides, as detailed for AHAB-2 (Gianaros *et al.*, 2014) and PIP (Gianaros *et al.*, 2017b).

AHAB-2 participants completed two versions of an fMRI facial expression, matching-to-sample task (see below). Subgroups of AHAB-2 and PIP participants also completed the same affective processing and responding task, which involved viewing IAPS stimuli (see below). Group- and individual-level fMRI data from the present report are available at NeuroVault (see Supplementary material; Gorgolewski *et al.*, 2015).

Pre-clinical atherosclerosis

AHAB-2 and PIP participants underwent CA-IMT assessments by trained sonographers using an Acuson Antares ultrasound device (Acuson-Siemens, Malvern, PA). Details on CA-IMT assessments are online (see Supplementary material). All CA-IMT values obtained for the left and right carotid arteries were averaged bilaterally to compute a grand mean CA-IMT, which served as the primary outcome variable.

The test-retest reliability of CA-IMT was determined in 14 participants in PIP who underwent ultrasonography twice (median 90 days apart, range 42–153 days). Across occasions, CA-IMT differed by −0.09 to 0.06 mm ($M = -0.005$, $SD = 0.042$ mm). The intraclass coefficient (ICC; ratio of variability between participants/total variability) was 0.82, indicating good reliability.

Facial expression-matching tasks

AHAB-2 participants completed two versions of a facial expression-matching task. The first was identical to the task used in our prior report on amygdala reactivity and CA-IMT (Gianaros *et al.*, 2008). In this task, participants completed four blocks of a facial expression-matching-to-sample condition, which was interleaved with five blocks of a shape-matching (sensorimotor) control condition. In the facial expression-matching condition, participants saw three same-sex faces in an array for each trial, all expressing either fear or anger. Participants chose one of the two faces at bottom that was identical to a center target at top. Each block consisted of six trials (three fear, three anger; three all-male, three all-female), and each trial lasted for 4 s (1.5, 3.5 and 5.5 s variable inter-trial interval; ITI). All images were in black and white and were drawn from the Pictures of Facial Affect (PFA) stimulus set (Ekman and Friesen, 1976). In the control condition, participants also matched-to-sample but instead used images of circles, vertical ellipses and horizontal ellipses. Each trio of shapes was shown for 4 s, with a 2 s ITI. The total task length was 6 min and 36 s, including 6 s for initial magnetic equilibration.

In the second version of the task, participants completed four blocks of facial expression, matching-to-sample trials (2 s trials; 60 s block length; variable ITI = 1, 3 and 5 s) and five interleaved blocks of sensorimotor control trials (2 s trials; 48 s block length; ITI = 2 s). In this version, however, blocks of trials were comprised of trios of angry, fearful, happy or neutral facial expressions (12 trials per block). All three faces for a given trial were matched for sex and emotional expression. Images in this task were shown in color and drawn from the NimStim Set of Facial Expressions (Tottenham, 2006). The total task length was 9 min and 12 s, including 6 s for initial magnetic equilibration. In both tasks, each block began with a 2 s cue: 'Match Faces' or 'Match Shapes'.

IAPS task

Subgroups of AHAB-2 and PIP participants completed an affective processing and responding task, which has been detailed previously (Gianaros *et al.*, 2014). Participants saw 30 unpleasant and 15 neutral IAPS images (Lang *et al.*, 2008). Participants were first trained and then instructed to (i) 'Look' and attend to images or (ii) 'Decrease' and change their thinking about the image to feel less negative. Trials were comprised of a 2-s cue ('Look' or 'Decrease'), followed by a 7-s IAPS image presentation. After image viewing, participants rated their emotional state ('How negative do you feel?') on a 5-point Likert-type scale in a 4-sec rating period (1 = neutral, 5 = strongly negative). A variable (1–3 s) rest period followed each rating period. The entire task duration was 11 min and 16 s (15 'Look neutral' trials; 15 'Look negative' trials; 15 'Decrease negative' trials). Images were presented such that no more than two identical trial types ('Look negative' or 'Decrease negative') were consecutive and no more than four unpleasant images were consecutive. Given the focus of this report (and for comparability to the facial expression tasks involving the passive viewing of affective stimuli), only 'Look neutral' and 'Look negative' trials were analyzed. Across AHAB-2 and PIP, unpleasant images for 'Look negative' trials overlapped by 87% (13/15 shared images) and neutral images by 13% (2/15 shared images).

As a manipulation check, we verified that unpleasant IAPS stimuli increased self-reported negative affect (Table 1), $t(337) = 61.80$, $P < 0.001$. The difference in negative affect ratings between 'Look negative' and 'Look neutral' trials (i.e. self-reported affective reactivity) was not statistically correlated with CA-IMT, $r(336) = -0.02$, $P = 0.76$. These behavioral data were thus omitted from further CA-IMT analyses.

E-Prime software (Psychology Software Tools, Sharpsburg, PA) was used to present stimuli and record behavioral responses in the facial expression and IAPS tasks. Table S1 lists image stimuli used for all tasks (see Supplementary material).

MRI data acquisition and analysis

Functional blood-oxygen-level-dependent (BOLD) images from AHAB-2 and PIP participants were collected on the same 3 Tesla Trio TIM whole-body scanner (Siemens, Erlangen, Germany), equipped with a 12-channel head coil. Data acquisition and pre-processing details are online (see Supplementary material).

In within-individual fMRI analyses, univariate general linear models (GLMs) were estimated to compute condition or event contrast maps that were later used for prediction analysis. Specifically, task conditions (or events) were modeled by rectangular waveforms convolved with the default hemodynamic response function in SPM12. For the facial expression-matching tasks, these regressors modeled blocks of face- and

Table 1. Analytic sample characteristics and descriptive statistics for study cohorts

	AHAB-2 $N = 458$	PIP $N = 159$
Characteristic		
Women (%)	52.4	50.3
Age (years)	42.6 ± 7.4	39.7 ± 6.4
Race (%)		
Caucasian/White	81.8	66.0
African-American	15.9	28.3
Multiracial/ethnic	2.2	5.6
Number of school years completed	16.9 ± 2.9	16.2 ± 3.3
Waist circumference (in)	35.5 ± 5.5	35.2 ± 5.3[f]
Total cholesterol (mg/dL)	199.8 ± 38.3[a]	182.8 ± 33.0[g]
Triglycerides (mg/dL)	109.4 ± 68.2[a]	95.5 ± 56.1[g]
HDL (mg/dL)	55.9 ± 15.0[a]	52.2 ± 16.0[g]
Glucose (mg/dL)	98.3 ± 11.2[a]	88.6 ± 8.8[g]
Clinic resting SBP (mmHg)	115.2 ± 11.1[b]	120.1 ± 10.5
Clinic resting DBP (mmHg)	72.2 ± 8.1[b]	72.0 ± 8.6
Accuracy in PFA faces task (%)	96.0 ± 14.0[c]	–
Accuracy in NimStim faces task (%)	95.9 ± 7.9[d]	–
NA ratings, unpleasant IAPS images	3.5 ± 0.7[e]	3.6 ± 0.6[f]
NA ratings, neutral IAPS images	1.1 ± 0.2[e]	1.3 ± 0.3[f]
Time between MRI and CA-IMT assessments (absolute days)	23.7 ± 47.0	58.1 ± 35.0
CA-IMT (mm)	0.638 ± 0.117[i]	0.609 ± 0.086[i]

Data are presented as percentage or mean ± standard deviation. AHAB-2, Adult Health and Behavior Project, Phase 2; PIP, Pittsburgh Imaging Project; HDL, high-density lipoproteins; SBP, systolic blood pressure; DBP, diastolic blood pressure; NA, negative affect and CA-IMT, carotid-artery intima-media thickness.
[a] $N = 457$.
[b] $N = 454$.
[c] $N = 424$.
[d] $N = 451$.
[e] $N = 183$.
[f] $N = 158$.
[g] $N = 155$.
[h] In AHAB-2, 49 participants completed the CA-IMT assessment on the same day as MRI; 177 completed CA-IMT the assessment on a separate day prior to MRI; 232 completed the CA-IMT assessment on a separate day following MRI. In PIP, all participants completed the CA-IMT assessment on a separate day prior to MRI.

shape-matching conditions. For the IAPS task, these regressors modeled events of the trial (i.e. cue, picture, rating period, rest). In each GLM, the six realignment parameters from pre-processing were included as nuisance regressors, and low-frequency artifacts were removed by a high-pass filter (128 s). Error variance was estimated and then weighted by restricted maximum likelihood estimation, as implemented in the RobustWLS toolbox, v4.0 (Diedrichsen and Shadmehr, 2005). Linear contrasts were then computed, including the 'Faces *vs* Shapes' contrast for the facial expression-matching tasks and 'Look negative *vs* Look neutral' contrast for the IAPS task. Main effects of the tasks were determined from these GLMs at the group (between-individual) level with whole-brain correction for multiple testing using a voxel-wise and false discovery rate threshold (0.05) combined with a voxel extent threshold of $k = 50$.

Missing data

Of the 490 AHAB-2 participants, 430 had complete fMRI data from the facial expression task using PFA faces and 453 using NimStim faces. Of the 430 with complete PFA data, 1 was excluded because of an anatomical abnormality, and 2 were excluded because of missing CA-IMT. Of the 453 with complete NimStim data, 2 were excluded because of missing CA-IMT, and 1 was excluded for insufficient brain coverage. AHAB-2 analyses were thus conducted on 427 participants with PFA data and 450 participants with NimStim data.

There were 180 AHAB-2 and 174 PIP participants with IAPS fMRI data. As noted, 15 people participated in AHAB-2 and PIP, and we used only their AHAB-2 data. Of the 354 total participants with IAPS fMRI data across the cohorts, 1 from AHAB-2 was excluded for insufficient brain coverage. Consequently, analyses were conducted on 179 AHAB-2 and 159 PIP participants with IAPS fMRI data.

In interim, there were 821 ($N = 490$ AHAB-2, $N = 331$ PIP) total individuals, but only 617 ($N = 458$ AHAB-2, $N = 159$ PIP) had complete and useable data for analysis, including useable fMRI data for one or more of the three affective tasks reported here. Table 1 summarizes demographic and other characteristics of the AHAB-2 and PIP analytic samples.

Multivariate prediction of CA-IMT

We used principal component regression combined with least absolute shrinkage and selection operator (hereafter, LASSO-PCR), as introduced for fMRI by Wager *et al.* (2011, 2013). LASSO-PCR was used to specifically test whether CA-IMT was predicted by BOLD signal responses evoked by the facial expression-matching tasks ('Faces *vs* Shapes') and by the IAPS task ('Look negative *vs* Look neutral'). To this end, evoked responses within gray matter voxels from all participant contrast maps served as the multivariate predictor, with CA-IMT as the dependent (outcome) variable. LASSO-PCR consisted of the following steps. To reduce voxel-wise predictor dimensionality and account for multicollinearity across voxels, the multivariate voxel-wise predictor matrix was first submitted to singular value decomposition (SVD). CA-IMT was then regressed onto the remaining principal components by LASSO using the 'lassoglm' function

in MATLAB (Tibshirani, 1996; Hastie *et al.*, 2005). In LASSO, estimated beta coefficients are subject to the L1 penalty (regularization). Applying this penalty, whose effect is modulated by the parameter lambda (λ), shrinks (penalizes) non-significant beta coefficients to zero to select predictive features (Efron et al., 2004; Zhao et al., 2009). Following feature selection, non-zero coefficients ($\hat{\beta}$) are projected back to voxel space via the SVD transformation matrix to produce a whole-brain weight map, $\hat{w}$. The dot product of this whole-brain weight map ($\hat{w}$) and a participant's contrast map of evoked signal change generates a predicted estimate of CA-IMT.

Nested and k-fold cross-validation was implemented to first optimize the shrinkage parameter λ in an 'inner loop' and then determine predictive generalizability of the multivariate weight maps in an 'outer loop'. Hence, to first identify the optimal shrinkage parameter, λ, and thus the number of principal components that best predicted CA-IMT, we used a five-fold cross-validation in the inner loop. In this way, participants were divided into training and validation samples by stratifying over the CA-IMT distribution. Within each cross-validation fold, LASSO-PCR was conducted on training samples using a sequence of 1000 λ values, and the performance of each λ was evaluated by calculating the average of the mean squared error (MSE) between predicted and observed CA-IMT across the validation samples. After identifying the optimal λ, the entire LASSO-PCR procedure was repeated using this λ on the entire inner loop sample, producing a whole-brain multivariate predictive pattern of CA-IMT.

To test the generalizability of the LASSO-PCR models and to generate unbiased estimates of predicted CA-IMT for each participant, we repeated the above process in an outer cross-validation loop. For the two facial expression tasks in the AHAB-2 cohort, the outer loop comprised a five-fold cross-validation. For the IAPS task, the outer loop comprised a two-fold cross-validation, which separated training and validation sets according to study membership (i.e. AHAB-2 *vs* PIP). The latter strategy was used to conservatively test for generalizability from one study sample to the other in view of observed cohort differences in CA-IMT (M CA-IMT in AHAB-2 = 0.638 mm; M CA-IMT in PIP = 0.609 mm; $t(336) = 2.10$, $P = 0.04$), prevalence of non-overlapping IAPS images (see Methods) and fMRI spatial signal coverage (mean percent coverage of all gray matter voxels in AHAB-2 = 86.27%; mean percent coverage in PIP = 93.59%; $t(336) = 29.83$, $P < 0.001$). Thus, the latter cross-validation procedure attempts to 'replicate' IAPS-based prediction findings for CA-IMT across the two cohorts (between AHAB-2 and PIP). Complete results and illustrations are available online (see Supplementary material).

The final predictive performance of a given weight map was summarized using several metrics describing the association between predicted and observed CA-IMT values concatenated across the k-folds of the outer loops (Forman and Scholz, 2010). Here, the similarity between predicted and observed values was summarized by the Pearson correlation coefficient and its corresponding 95% confidence interval (CI) and P-value. The discrepancy between predicted and observed values was calculated using mean absolute error (MAE). Following guidelines for predictive modeling (Poldrack *et al.*, 2019; Scheinost *et al.*, 2019), variance in observed values explained by predicted values (R^2) was calculated by inserting the out-of-sample predictions in the sums of squares formulation. To aid in interpreting results that did not meet conventional statistical significance, we computed Bayes factors (BF10, BF01) using the 'BayesFactors' package (v0.9.12–4.2; Morey and Rouder, 2011) in R (R-Core-Team, 2014). BF10 values reflect the probability of the alternative hypothesis, relative to the null. BF01 values reflect the inverse of BF10 values, corresponding to evidence for the null relative to the alternative hypotheses.

To identify which particular voxels reliably contributed to a given multivariate weight map, we used bootstrap resampling (1000 iterations) and repeated the LASSO-PCR and k-fold cross-validation steps. P-values for voxel-wise estimates were then computed by non-parametric percentile methods, and the bootstrapped multivariate weight maps were thresholded at $P < 0.05$ (two-tailed) with an extent threshold of $k = 50$ voxels.

LASSO-PCR and nested cross-validation procedures were implemented using in-house MATLAB code adapted from Wager and colleagues (Wager *et al.*, 2011, 2013). All code is available online (see Supplementary material).

Ancillary tests of amygdalar contributions

Amygdala functionality has been implicated in CVD risk (see Introduction). This raises the question of whether amygdala activity is necessary or sufficient to predict CA-IMT. To address this question, we repeated the above nested cross-validated LASSO-PCR steps for each affective task, first restricting all predictor voxels to a bilateral anatomical mask of the amygdala. Next, we performed a 'virtual lesion' analysis, wherein all voxels of the amygdala mask were excluded from nested cross-validation. The anatomical mask included the left and right amygdalae of the automated anatomical labeling atlas (Tzourio-Mazoyer *et al.*, 2002) in the Wake Forest University PickAtlas Toolbox (Maldjian *et al.*, 2003).

Ancillary tests of discriminant prediction

We further explored whether CA-IMT could be predicted by an entirely different brain pattern that statistically explains self-reports of negative affect evoked by unpleasant IAPS stimuli, namely, the Picture-Induced Negative Emotion Signature (PINES; Chang *et al.*, 2015). If so, then this could suggest that brain patterns derived here are not uniquely predictive of pre-clinical atherosclerosis but rather interchangeable or redundant with brain correlates of self-reported negative affect.

Ancillary tests of 'confounders'

Demographic, anthropometric and biological factors were explored as effect moderators or 'confounders' that may impact primary study findings. These included tests of age and sex as moderators, as well tests of age, sex and components of the metabolic syndrome as covariates. For the latter and following prior work (Gianaros *et al.*, 2017a), a standard composite cardiometabolic risk (CMR) score was computed by z-scoring systolic BP, waist circumference and fasting concentrations of glucose, HDL levels and triglycerides and then averaging the z-scores (HDL signs reversed).

Psychometric properties of task-related fMRI activity

To assess the internal consistency of fMRI activity changes evoked by tasks, we executed the split-half method in line with procedures of Infantolino *et al.* (2018). Specifically, for each participant, GLM analyses were estimated, and contrast images were generated separately using approximate partitions of the first and second half of the BOLD signal data from each

task. For the PFA-based faces task, there were four expression-matching blocks and five shape-matching blocks. The last block of shape-matching trials was not included, so that the first and second partitions of the data each had two face- and shape-matching blocks. For the NimStim-based faces task, there were four expression-matching blocks and five shape-matching blocks. Again, the last block of shape-matching trials was not modeled. For the IAPS task, there were 45 trials that could not be partitioned equally in a conventional split-half analysis because of the nature of the event-related design and its stimulus ordering. As a result, the fMRI run was partitioned into the first 23 trials and the last 22 trials (resulting in 10 *vs* 5 'Look negative' and 7 *vs* 8 'Look neutral' trials, respectively).

We first computed the split-half, internal consistency of amygdala activity within each task by extracting the average contrast value within the bilateral AAL amygdala mask, and we examined the reliability of the extracted parameter estimates using the Spearman–Brown (SB) correction method. For completeness of reporting, we then generated voxel-wise internal consistency maps for each task. These voxel-wise maps are available online at NeuroVault (see also Supplementary material). Finally, we computed the internal consistency of the weight maps generated by LASSO-PCR to predict CA-IMT. To this end, we computed the dot product between each whole-brain weight map ($\hat{w}$) with all pairs of participant contrast maps generated from the split-half procedure, which effectively tested for the consistency of CA-IMT prediction within participants (Woo and Wager, 2016).

Results

Main effects of the facial expression-matching tasks

The 'Faces *vs* Shapes' contrasts for the facial expression-matching tasks using stimuli from the PFA and NimStim sets showed that both tasks engaged an ensemble of cortical and subcortical brain regions in the AHAB-2 cohort (Figure 1a and b and Supplementary Tables S2–S3). Although both tasks positively engaged the amygdala on average (Figure 1a and b), the internal consistency metrics for extracted amygdala activation values were poor for tasks using PFA (0.27) and NimStim (0.11) facial expressions. The latter observations match those of prior reports indicating poor psychometric properties of extracted amygdala activation values, as evoked by facial expression-matching-to-sample tasks (Infantolino *et al.*, 2018; Elliott *et al.*, 2020). However, we note that on a voxel-wise basis, internal consistency values varied appreciably across the brain for both face-matching tasks, with some areas (e.g. in visual cortex) exhibiting moderate-to-good internal consistency (interactive maps available at NeuroVault; see also Supplementary material).

Main effects of the IAPS task

The 'Look negative *vs* Look neutral' contrast revealed that viewing unpleasant IAPS images also engaged a distributed ensemble of brain regions known to respond to complex visual affective scenes, including a positive engagement of the amygdala and areas of the medial pre-frontal, anterior cingulate and anterior insular cortices. Figure 1c and Supplementary Table S4 summarize these main effects, as aggregated across the AHAB-2 and PIP cohorts ($N = 338$). Across participants, the internal consistency of extracted activation values from the amygdala was comparable to those for the facial expression-matching tasks (0.24). As observed for the facial expression-matching tasks, there was wide variability in internal consistency on a voxel-wise basis (maps available at NeuroVault; see also Supplementary material).

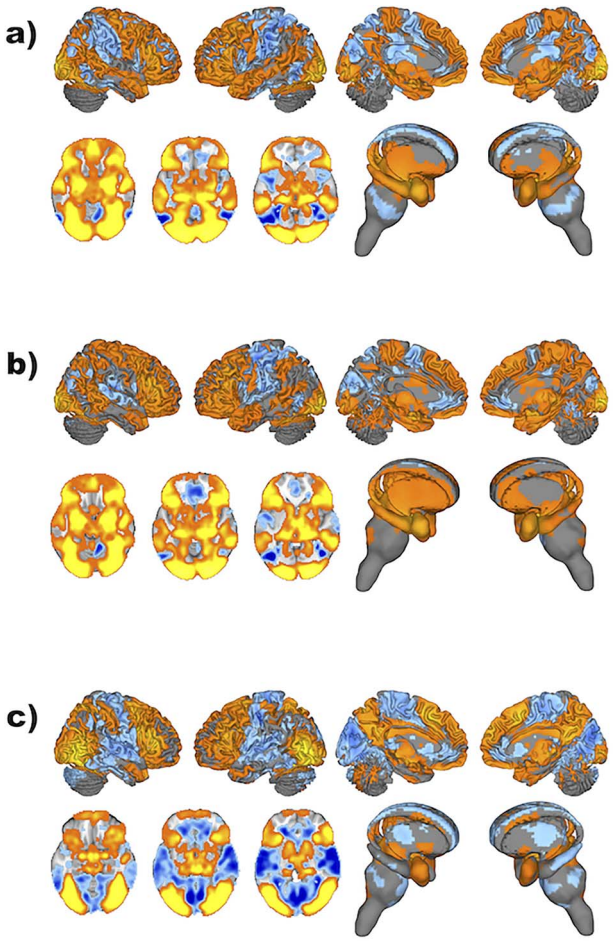

Fig. 1. Color-scaled T-maps of brain areas exhibiting significant BOLD signal changes for the contrasts of Faces *vs* Shapes and Look negative *vs* Look neutral are shown for the facial expression-matching task employing PFA (A) and NimStim faces (B), as well as IAPS images (C), respectively. Maps in A–C correspond to statistical parametric T-maps, shown at a false discovery rate (FDR) threshold of 0.05 to control for multiple statistical testing across voxels, with an extent threshold of $k > 50$ voxels. Axial planes correspond to z coordinates −16, −8 and 0. Warmer colors (orange/yellow) reflect activation, whereas cooler colors (blue) reflect deactivation. Clusters are described in the Supplementary material.

Prediction of CA-IMT from whole-brain patterns evoked by the facial expression-matching tasks

PFA-based prediction. Using cross-validated LASSO-PCR, we found that CA-IMT was predicted by a model trained on the contrast of 'Faces *vs* Shapes' (inclusive of angry and fearful faces) from the PFA facial expression-matching task, optimal $\lambda = 0.0113$, 24 principal components retained, MSE = 0.0137. As shown in Figure 2a, nested cross-validation showed that CA-IMT predicted by the whole-brain multivariate brain pattern correlated with observed CA-IMT, $r(425) = 0.13$, 95% CI = 0.04–0.23, $P = 0.005$, MAE = 0.089, $R^2 = 0.014$, BF10 = 5.16, BF01 = 0.19. The internal consistency of the PFA-based weight map was 0.73. Figure 3a illustrates brain areas within the whole-brain multivariate pattern that consistently predicted CA-IMT across individuals in holdout validation sample testing, as determined by bootstrapping. We reiterate that a whole-brain pattern was

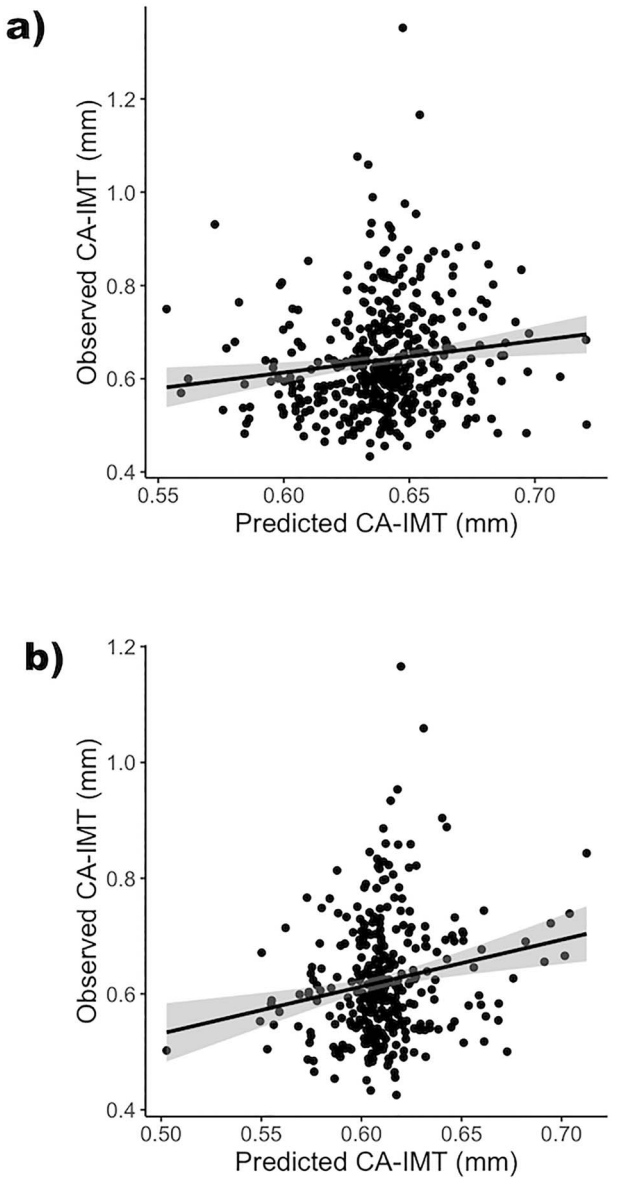

Fig. 2. A comparison of predicted *vs* observed CA-IMT using cross-validated LASSO-PCR in the (A) PFA-based facial expression-matching task and (b) IAPS task.

used for cross-validated prediction; however, it is noteworthy from the lower right panel of Figure 3a that the predictive contributions of the amygdala were mostly *negative* (94 or 20% negative *vs* 17 or 3.6% positive voxel weights out of 468 possible voxels within the amygdala mask). The latter indicates that there were more voxels within the amygdala where *lower* evoked activity predicted *higher* CA-IMT.

When cross-validated LASSO-PCR was restricted to voxels within the amygdala, CA-IMT continued to be predicted across individuals—albeit with a smaller effect size, $r(425) = 0.10$, 95% CI = 0.003–0.19, $P = 0.044$, MAE = 0.010, $R^2 = 0.006$, BF10 = 0.84, BF01 = 1.19. And, in a 'virtual lesion' analysis in which we applied the amygdala mask to omit this region from the whole-brain LASSO-PCR and nested cross-validation steps, we continued to observe an association between predicted and observed CA-IMT, $r(425) = 0.13$, 95% CI = 0.04–0.22, $P = 0.007$, MAE = 0.090, $R^2 = 0.014$, BF10 = 4.16, BF01 = 0.24. The latter findings suggest that the amygdala was not necessary for predicting CA-IMT from the whole-brain predictive pattern.

The relationship between predicted and observed CA-IMT was not moderated by age ($\beta = 0.04$, SE = 0.04, $P = 0.340$, BF10 = 0.16, BF01 = 6.25) or sex ($\beta = 0.06$, SE = 0.05, $P = 0.187$, BF10 = 0.43, BF01 = 2.33) when the latter were added as interaction terms. In tests of confounding influences, however, covariate adjustment for age, sex and the composite cardiometabolic risk score demonstrated that predicted and observed CA-IMT no longer correlated at a conventional statistical threshold of $P < 0.05$ ($\beta = 0.03$, SE = 0.04, $t(422) = 0.80$, $P = 0.424$, BF10 = 0.14, BF01 = 7.15).

Lastly, in a test of discriminant prediction, applying the PINES brain pattern for self-reported negative affect to the PFA contrast maps of 'Faces *vs* Shapes' failed to statistically predict CA-IMT, $r(425) = -0.06$, 95% CI = –0.15 to 0.04, $P = 0.22$, MAE = 1.608, $R^2 < 0$, BF10 = 0.24, BF01 = 4.16. This suggests that multivariate brain patterns for predicting self-reported negative affect *vs* CA-IMT are dissociable and not redundant for the PFA task paradigm.

NimStim-based prediction. Using cross-validated LASSO-PCR, we found that CA-IMT was not reliably predicted by whole-brain patterns revealed by the 'Faces *vs* Shapes' contrast (inclusive of angry, fearful, happy and neutral facial expressions) from the facial expression-matching task using NimStim images. This null result was reflected in predicted CA-IMT values that did not statistically correlate with observed CA-IMT, $r(448) = 0.04$, 95% CI = –0.06 to 0.13, $P = 0.354$, MAE = 0.088, $R^2 < 0$, BF10 = 0.17, BF01 = 5.88. Similar findings were revealed by *post-hoc* tests of whether the specific contrast of 'Fear and Anger *vs* Shapes' predicted CA-IMT, $r(448) = 0.07$, 95% CI = –0.02 to 0.16, $P = 0.127$, MAE = 0.088, $R^2 < 0$, BF10 = 0.34, BF01 = 2.88 (full results available in the Supplementary material). These *post-hoc* tests were executed for a more direct comparison of findings from the PFA-based facial expression paradigm, which included only expressions of fear and anger. Because a reliable whole-brain pattern of brain activity predictive of CA-IMT could not be generated using the NimStim-based task, we did not explore ancillary moderation, confounder, internal consistency or PINES tests.

Prediction of CA-IMT from whole-brain activity patterns evoked by IAPS images

Using cross-validated LASSO-PCR, we found that CA-IMT was predicted by a whole-brain multivariate pattern derived from the 'Look negative *vs* Look neutral' contrast based on the IAPS task, optimal $\lambda = 0.0049$, 113 principal components retained, MSE = 0.0099. As revealed by nested cross-validation and shown in Figure 2b, predicted and observed CA-IMT values were statistically correlated, $r(336) = 0.19$, 95% CI = 0.10–0.28, $P < 0.001$, MAE = 0.076, $R^2 = 0.023$, BF10 = 47.10, BF01 = 0.02. The internal consistency of the multivariate IAPS pattern was 0.82. Figure 3b shows brain areas within the multivariate pattern that consistently predicted CA-IMT, as determined by bootstrapping. We note that surviving predictive weights within the amygdala were uniformly negative (90 or 19% negative *vs* 0 positive voxel weights out of 468 possible voxels), again indicating that *lower* evoked activity predicted *higher* CA-IMT.

When the cross-validated LASSO-PCR procedure was restricted to the anatomical mask of the amygdala, the LASSO-PCR model trained on one study cohort failed to generalize to predict CA-IMT in the other study cohort. Moreover, after excluding voxels within the amygdala from LASSO-PCR in a 'virtual lesion' analysis, we continued to observe an association

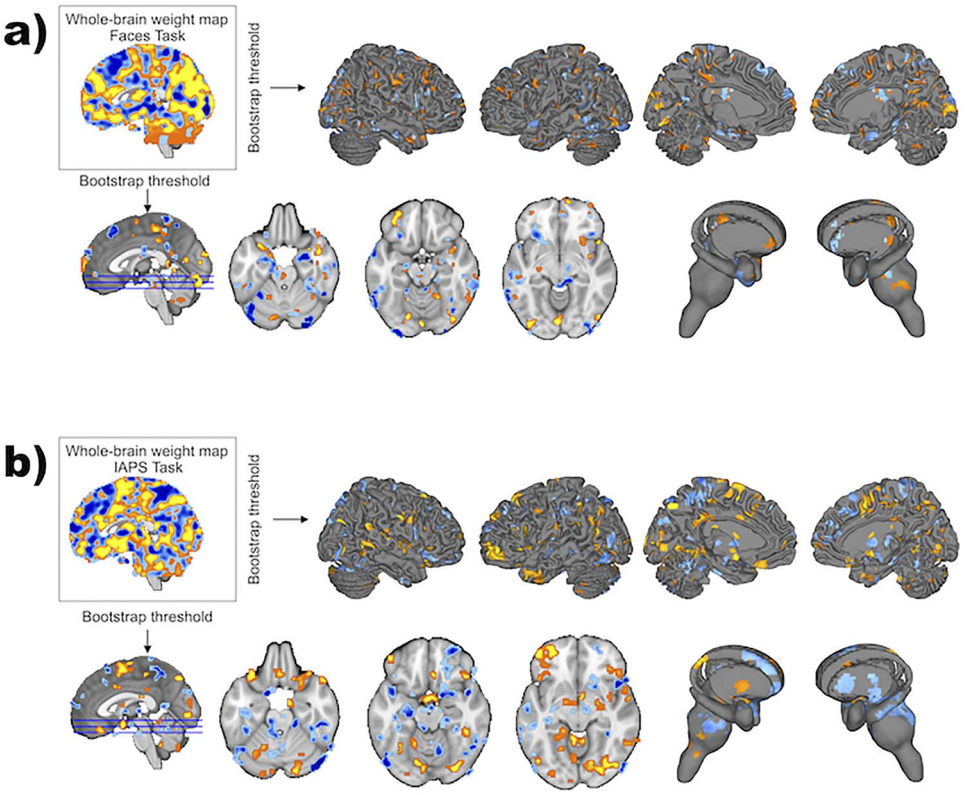

Fig. 3. Whole-brain weight maps used to predict CA-IMT from the (a) PFA-based facial expression-matching task and (b) IAPS task. The maps are thresholded to display voxels which reliably contributed to prediction. Here, the maps are shown at a threshold of $P < 0.05$ *and* $k > 50$ *voxels*, based on bootstrapping (1000 iterations). Axial planes correspond to z coordinates −16, −8 and 0. Warmer colors (orange/yellow) reflect a positive pattern weight, whereas cooler colors (blue) reflect a negative weight.

between predicted and observed CA-IMT across participants, $r(336) = 0.19$, 95% CI = 0.10–0.28, $P = 0.001$, MAE = 0.076, $R^2 = 0.022$, BF10 = 45.70, BF01 = 0.02. The latter findings indicate that amygdala activity was neither necessary nor sufficient to predict CA-IMT.

In a test of discriminant prediction, applying the PINES pattern for predicting self-reported negative affect to 'Look negative *vs* Look neutral' contrast maps failed to predict CA-IMT, $r(336) = 0.04$, 95% CI = –0.07 to 0.15, $P = 0.442$, MAE = 1.023, $R^2 < 0$, BF10 = 0.17, BF01 = 5.88, again suggesting that brain patterns for self-reported negative affect *vs* CA-IMT are dissociable.

The relationship between predicted and observed CA-IMT was not moderated by age ($\beta = 0.07$, SE = 0.05, $P = 0.155$, BF10 = BF10 = 0.33, BF01 = 3.03) or sex ($\beta = -0.05$, SE = 0.05, $P = .384$, BF10 = 0.29, BF01 = 3.45). And in contrast to findings from the facial expression task using PFA stimuli, adjustment for age, sex and the composite index of cardiometabolic risk demonstrated that predicted and observed CA-IMT continued to correlate, $\beta = 0.17$, SE = 0.04, $t(333) = 3.84$, $P < 0.001$, BF10 = 147.81, BF01 < 0.01.

Discussion

This study tested whether whole-brain fMRI activity patterns evoked by three affective information processing tasks would reliably predict individual differences in CA-IMT, a vascular marker of pre-clinical atherosclerosis and CVD risk. First, as revealed by multivariate, machine learning and cross-validation methods, ~1.4% of the variance in CA-IMT across individuals was explained by a whole-brain pattern that was trained on fMRI activity elicited by viewing facial expressions of emotion (anger and fear). These expressions were presented in a canonical matching-to-sample task using PFA stimuli (Figures 2a and 3a). Although the latter predictive relationship between fMRI activity and CA-IMT was observed in a large cohort of individuals ($N = 427$) through k-fold cross-validation, it failed to persist after accounting for age, sex and known CVD risk factors. Second, CA-IMT was not reliably predicted by a whole-brain pattern elicited by viewing angry, fearful, happy and neutral facial expressions in a similar matching-to-sample task using NimStim stimuli ($N = 450$; see Supplementary material). Comparable findings were observed when models were trained only on fMRI activity patterns evoked by angry and fearful NimStim facial expressions (see Supplementary material). Third, ~2.3% of the variance in CA-IMT was explained by a whole-brain pattern trained on fMRI activity elicited by viewing IAPS images of unpleasant affective scenes (Figures 2b and 3b). The latter predictive relationship (i) generalized across two different study samples (N's of 179 in AHAB-2 and 159 in PIP) and (ii) persisted after accounting for age, sex and known risk factors for CVD. Fourth, aggregate evidence across all predictive models was largely inconsistent with (or opposite to) prior findings suggesting that *greater* amygdala reactivity to affective information relates to *greater* pre-clinical atherosclerosis, as measured by CA-IMT (Gianaros *et al.*, 2008). Rather, multivariate associations between amygdala activity and CA-IMT were largely *negative* when present. Lastly, CA-IMT was not statistically associated with self-reports of negative affect induced by viewing unpleasant affective scenes or a previously established brain pattern (i.e. the PINES) that predicts self-reported negative affect (Chang *et al.*,

2015), suggesting dissociable neural correlates of self-reported negative affect and vascular markers of CVD risk. Collectively, the present findings provide novel evidence for neural correlates of CVD risk that extend beyond localized amygdala activity to include multivariate and generalizable patterns that are distributed across other brain systems for affective processing. As described below, the interpretation and predictive strength of these multivariate neural correlates may depend on their psychometric properties, the influence of other cardiovascular risk factors and perhaps the specific affective cues used to evoke neural activity.

To elaborate, recent evidence suggests that amygdala functionality may associate with clinically relevant cardiovascular endpoints and surrogate markers of CVD risk (e.g. Tawakol *et al.*, 2017; Ishai *et al.*, 2019; Osborne *et al.*, 2019). Pre-dating the latter evidence were findings that greater amygdala activity to facial expressions of fear and anger was associated with a greater severity of pre-clinical atherosclerosis, suggesting that amygdala 'hyperactivity' evoked by affective cues (facial expressions of emotion) may comprise a neural correlate of CVD risk (Gianaros *et al.*, 2008). Here, we administered the same facial expression-matching-to-sample fMRI task that we used previously, wherein participants matched faces depicting anger and fear derived from the PFA stimulus set. This task was complemented by another facial expression-matching task that included not only angry and fearful facial expressions but also happy and neutral expressions that were all drawn from a different and more recently developed stimulus set (NimStim). The latter NimStim-based task was administered in an attempt to test whether any findings derived from the PFA-based task generalized to a broader range of affectively salient expressions and human models.

Using the PFA-based task, we found that a *whole-brain* activity pattern predicted CA-IMT in final cross-validation testing ($R^2 = 0.014$). This cross-validated and predictive relationship, however, did not depend on the contributions of the amygdala in a 'virtual lesion' analysis. Nor did the predictive relationship derived from the whole-brain pattern remains statistically significant following covariate control for age, sex and known cardiovascular risk factors. In addition, the predictive weights within the amygdala in both whole-brain and ROI-based analyses were largely *negative*, not positive—meaning that *greater* CA-IMT was predicted by *lower* levels of evoked amygdala activity. The latter observations disagree with the positive associations we previously reported between amygdala activation to angry and fearful facial expressions and CA-IMT using mass-univariate and ROI methods (Gianaros *et al.*, 2008). Moreover, the NimStim-based task failed to produce a generalizable multivariate brain pattern that predicted CA-IMT using either all facial expressions or only a subset expressing anger and fear. One reason why fMRI activity from these two facial expression-matching tasks did not consistently relate to CA-IMT may be due to their relatively limited psychometric properties and, thus, unclear suitability for individual difference research. The latter conclusion is supported not only by the present findings but also those reported by Infantolino *et al.* (2018) and summarized by meta-analysis (Elliott *et al.*, 2020). Indeed, *post-hoc* exploratory findings (Figure S5) suggested that internal consistency values were related to predictive performance on a voxel-wise basis across all tasks used in the present study. As specifically shown in Figures S5 (panels e and f), voxels exhibiting lower internal consistency values tended to exhibit lower prediction weights. Consequently, internal consistency appeared to 'constrain' prediction weights in a manner that accords with classical test theory (Cohen *et al.*, 2003). In these regards, the psychometric characteristics of fMRI activity patterns evoked by affective and other task paradigms should be considered in individual differences research on CVD risk.

Compared to findings from the facial expression-matching tasks, a LASSO-PCR model trained on whole-brain activity evoked by viewing complex and unpleasant IAPS stimuli in one study cohort generalized to predict CA-IMT in a different study cohort, with a relatively larger coefficient of determination ($R^2 = 0.023$). Viewing unpleasant IAPS stimuli also engaged a broad ensemble of brain areas implicated in affective processing and visceral control functions relevant to CVD risk, including the insula, hypothalamus, brainstem and areas of the anterior cingulate and medial pre-frontal cortices (Figure 1c). Moreover, the multivariate (i.e. whole-brain) predictive pattern of activity evoked by the IAPS task exhibited reasonable psychometric properties, particularly relative to those observed for the facial expression-matching tasks. Indeed, the multivariate IAPS pattern predictive of CA-IMT exhibited an internal consistency value of 0.82, approximating the test-retest reliability (ICC) value observed in one of our samples (PIP) for CA-IMT itself (0.82). It is notable that this predictive model continued to account for CA-IMT above and beyond canonical CVD risk factors in final cross-validation testing (age, sex and a composite cardiometabolic risk score).

Also notable from Figure 3b is that regions most consistently predictive of CA-IMT within the whole-brain pattern encompassed those implicated in linking affective processes (and negative affect in particular) to CVD risk via downstream influences over health behaviors and systemic physiology (Kraynak *et al.*, 2018a), including predictive contributions from the insula, hypothalamus, brainstem and areas of the anterior cingulate and medial pre-frontal cortices (Figure 3b; Supplementary Table S6). However, the amygdala appeared neither necessary nor sufficient for predicting CA-IMT across individuals in ROI and 'virtual lesion' analyses within the context of the IAPS task. Lastly, viewing unpleasant IAPS stimuli induced a mean increase in self-reported negative affect across individuals. These self-reports, however, were insufficient as explanatory predictors of CA-IMT, as was a multivariate brain pattern that predicts self-reported negative affect (i.e. the PINES pattern). These observations again suggest a dissociation between the neural correlates of the subjective experience of negative emotion and the neural correlates of CVD risk (e.g. as measured at the level of the peripheral vasculature by CA-IMT). Viewing complex and unpleasant affective scenes may thus not only induce negative affect but also a unique pattern of brain activity that exhibits a predictive relationship (albeit of small effect size) with CA-IMT.

Inferences from the present findings are constrained by study design and sample characteristics, as well as related methodological limitations. First, our cross-sectional observations preclude causal inference. For example, in a health neuroscience framework (Erickson *et al.*, 2014), it may be that the IAPS-based multivariate brain pattern that predicted CA-IMT corresponds to a brain phenotype that reflects a link between negative affective processes and CVD risk via top-down (brain-to-body or brain-to-behavior) pathways. These pathways could encompass individual differences in affect-related neural influences on peripheral physiology and health behaviors. At the same time, pre-clinical cardiovascular pathophysiology could plausibly influence patterns of brain activity that predicted CA-IMT via bottom-up (body or behavior-to-brain) pathways, such as via the ascending (afferent) influences of immune and autonomic

input to the brain that in turn bias how individuals process and respond to affective cues (Kraynak *et al.*, 2018a, b). Second, the study samples were predominately of European ancestry, well-educated and limited to people free of major chronic illnesses and medication regimens that could have confounded interpretations of CA-IMT and related CVD risk metrics. As a result, the relevance of our findings to demographically diverse individuals and clinical populations is unclear. However, our whole-brain maps are publicly available and could be applied in other populations and tested as predictors of clinical outcomes or other markers of pre-clinical CVD. Third, we adopted an omnibus training and testing methodology, collapsing across facial expressions of diverse emotions and IAPS stimuli depicting a range of affective scenes to produce contrast images of 'Faces *vs* Shapes' and 'Negative *vs* Neutral' activity patterns. This was done without an a priori focus on affect- or content-specific predictive testing. Using publicly available contrast images from the present study, it would be feasible for others to generate and test more granular affective predictive maps for CA-IMT. Fourth, it may be that metrics of *resting* metabolic activity within brain systems for affective processes or even distributed network (e.g. intrinsic, resting-state or task-based connectivity) metrics may hold methodological and possibly psychometric advantages than the task-based activation metrics employed here, as indicated by work on CVD risk and resting metabolic activity within the amygdala (Tawakol *et al.*, 2017). Finally, we may have observed differential predictions of CA-IMT across tasks because of design characteristics and specific affective cues. Both the face-processing and IAPS tasks involved the passive encoding of salient affective cues; however, only the IAPS task employed complex emotional and naturalistic scenes that would plausibly evoke an affective experience (e.g. as verified in the present study by a mean increase in negative affect).

Other design differences may likewise explain divergent findings across the face-processing and IAPS tasks. For example, both face-processing tasks relied on blocked stimulus presentations, with repeated exposures to some cues (or human models) that were presented for 2–4 s. By contrast, the IAPS task used an event-related design, with no repeated exposures to affective cues and longer stimulus presentation times (7 s). In addition to differences in stimulus content, novelty and the complexity of the affective cues (faces *vs* scenes), there were notable differences in the control conditions used to create fMRI activation maps (shapes *vs* scenes). Together, these paradigmatic differences could have impacted how affective cues were encoded and experienced, thus impacting manifest psychometric characteristics of relative changes fMRI activity patterns used for predictive modeling. In extension, it is notable that metrics reflecting individual differences in the habituation of task-evoked neural responses to repeated or sequential affective cues (e.g. within the amygdala) may hold promise for identifying replicable brain phenotypes for cardiovascular risk relative to conventional and directional activity changes studied here (Plichta *et al.*, 2014). An important future direction will be to validate task paradigms and fMRI activity metrics that maximize psychometric properties and utility for individual difference research.

To close, individual differences in emotion and affect have been studied in association with risk for CVD, historically at the level of peripheral physiology, behavior and self-report. This line of inquiry has been extended to the level of the brain in health neuroscience, especially within the past decade. While there has been a strong conceptual and empirical focus on the amygdala as key brain system for CVD risk, the present findings support a broader focus on distributed neural systems in association with markers of CVD risk and early (pre-clinical) pathophysiology. The present findings also underscore the relevance of multivariate and cross-validation methodologies, as well as psychometric characteristics of fMRI tasks, for building predictive models that characterize replicable affective neural correlates of CVD risk.

Supplementary data

Supplementary data are available at *SCAN* online. Code for analysis and group- and individual-level fMRI data are available at GitHub (https://github.com/CoAxLab/IMT_manuscript) and NeuroVault (https://neurovault.org/collections/EBPXRZTX/).

Funding

Research reported in this publication was supported by the National Heart, Lung, and Blood Institute of the National Institutes of Health under Award Numbers P01HL040962 and R01089850. The content is solely the responsibility of the authors and does not necessarily represent the official views of the National Institutes of Health.

Conflict of interest

None declared.

References

Baber, U., Mehran, R., Sartori, S., *et al.* (2015). Prevalence, impact, and predictive value of detecting subclinical coronary and carotid atherosclerosis in asymptomatic adults: the BioImage study. *Journal of the American College of Cardiology*, **65**(11), 1065–74. doi: 10.1016/j.jacc.2015.01.017.

Chang, L.J., Gianaros, P.J., Manuck, S.B., Krishnan, A., Wager, T.D. (2015). A sensitive and specific neural signature for picture-induced negative affect. *PLoS Biology*, **13**(6), e1002180. doi: 10.1371/journal.pbio.1002180.

Cohen, J., Cohen, P., West, S.G., Aiken, L.S. (2003). *Applied Multiple Regression/Correlation Analysis for the Behavioral Sciences*, 3rd edn, Mahwah, N.J.: Lawrence Erlbaum Associates.

Davidson, K.W., Alcantara, C., Miller, G.E. (2018). Selected psychological comorbidities in coronary heart disease: challenges and grand opportunities. *The American Psychologist*, **73**(8), 1019–30. doi: 10.1037/amp0000239.

DeSteno, D., Gross, J.J., Kubzansky, L. (2013). Affective science and health: the importance of emotion and emotion regulation. *Health Psychology*, **32**, 474–86.

Diedrichsen, J., Shadmehr, R. (2005). Detecting and adjusting for artifacts in fMRI time series data. *NeuroImage*, **27**(3), 624–34. doi: 10.1016/j.neuroimage.2005.04.039.

Efron, R., Hastie, T., Johston, I., & Tibshirani, R. (2004). Least Angle Regression. *Annals of Statistics*, **32**, 407–499.

Eisenbarth, H., Chang, L.J., Wager, T.D. (2016). Multivariate brain prediction of heart rate and skin conductance responses to social threat. *The Journal of Neuroscience*, **36**(47), 11987–98. doi: 10.1523/JNEUROSCI.3672-15.2016.

Ekman, P., Friesen, W.V. (1976). *Pictures of Facial Affect*, Palo Alto: Consulting Psychologists Press.

Elliott, M.L., Knodt, A.R., Ireland, D., *et al.* (2020). Poor test-retest reliability of task-fMRI: new empirical evidence and a meta-analysis. *Psycholgoical Science*. doi: 10.1101/681700.

Erickson, K.I., Creswell, J.D., Verstynen, T.D., Gianaros, P.J. (2014). Health neuroscience: defining a new field. *Current Directions in Psychological Science*, **23**, 446–53.

Forman, G., Scholz, M. (2010). Apples-to-apples in cross-validation studies: pitfalls in classifier performance measurement. *SIGKDD Explor. Newsl.*, **12**, 49–57.

Gianaros, P.J., Jennings, J.R. (2018). Host in the machine: a neurobiological perspective on psychological stress and cardiovascular disease. *The American Psychologist*, **73**(8), 1031–44. doi: 10.1037/amp0000232.

Gianaros, P.J., Wager, T.D. (2015). Brain-body pathways linking psychological stress and physical health. *Current Directions in Psychological Science*, **24**, 313–21.

Gianaros, P.J., Hariri, A.R., Sheu, L.K., Muldoon, M.F., Sutton-Tyrrell, K., Manuck, S.B. (2008). Preclinical atherosclerosis covaries with individual differences in reactivity and functional connectivity of the amygdala. *Biological Psychiatry*, **65**, 943–50. doi: 10.1016/j.biopsych.2008.10.007.

Gianaros, P.J., Marsland, A.L., Kuan, D.C., *et al.* (2014). An inflammatory pathway links atherosclerotic cardiovascular disease risk to neural activity evoked by the cognitive regulation of emotion. *Biological Psychiatry*, **75**, 738–45. doi: 10.1016/j.biopsych.2013.10.012.

Gianaros, P.J., Kuan, D.C., Marsland, A.L., *et al.* (2017a). Community socioeconomic disadvantage in midlife relates to cortical morphology via neuroendocrine and cardiometabolic pathways. *Cerebral Cortex*, **27**, 460–73. doi: 10.1093/cercor/bhv233.

Gianaros, P.J., Sheu, L.K., Uyar, F., *et al.* (2017b). A brain phenotype for stressor-evoked cardiovascular reactivity. *Journal of the American Heart Association*, **6**, e006053. doi: 10.1161/JAHA.117.006053.

Ginty, A.T., Kraynak, T.E., Fisher, J.P., Gianaros, P.G. (2017). Cardiovascular and autonomic reactivity to psychological stress: neurophysiological substrates and links to cardiovascular disease. *Autonomic Neuroscience*, **207**, 2–9. doi: 10.1016/j.autneu.2017.03.003.

Gorgolewski, K.J., Varoquaux, G., Rivera, G., *et al.* (2015). Neuro Vault.org: a web-based repository for collecting and sharing unthresholded statistical maps of the human brain. *Frontiers in Neuroinformatics*, **9**, 8. doi: 10.3389/fninf.2015.00008.

Goyal, A., Dey, A.K., Chaturvedi, A., *et al.* (2018). Chronic stress-related neural activity associates with subclinical cardiovascular disease in psoriasis: a prospective cohort study. *JACC: Cardiovascular Imaging*. doi: 10.1016/j.jcmg.2018.08.038.

Hastie, T., Tibshirani, R., Friedman, J., Franklin, J. (2005). The elements of statistical learning: data mining, inference and prediction. *The Mathematical Intelligencer*, **27**, 83–5.

Infantolino, Z.P., Luking, K.R., Sauder, C.L., Curtin, J.J., Hajcak, G. (2018). Robust is not necessarily reliable: from within-subjects fMRI contrasts to between-subjects comparisons. *NeuroImage*, **173**, 146–52. doi: 10.1016/j.neuroimage.2018.02.024.

Ishai, A., Osborne, M.T., Tung, B., *et al.* (2019). Amygdalar metabolic activity independently associates with progression of visceral adiposity. *The Journal of Clinical Endocrinology and Metabolism*, **104**(4), 1029–38. doi: 10.1210/jc.2018-01456.

Krantz, D.S., McCeney, M.K. (2002). Effects of psychological and social factors on organic disease: a critical assessment of research on coronary heart disease. *Annual Review of Psychology*, **53**, 341–69. doi: 10.1146/annurev.psych.53.100901.135208.

Kraynak, T.E., Marsland, A.L., Gianaros, P.J. (2018a). Neural mechanisms linking emotion with cardiovascular disease. *Current Cardiology Reports*, **20**(12), 128. doi: 10.1007/s11886-018-1071-y.

Kraynak, T.E., Marsland, A.L., Wager, T.D., Gianaros, P.J. (2018b). Functional neuroanatomy of peripheral inflammatory physiology: a meta-analysis of human neuroimaging studies. *Neuroscience and Biobehavioral Reviews*, **94**, 76–92. doi: 10.1016/j.neubiorev.2018.07.013.

Lang, P.J., Bradley, M.M., Cuthbert, B.N. (2008). International affective picture system (IAPS): Affective ratings of pictures and instruction manual. *Technical Report*. **A-8**. University of Florida, Gainesville, FL.

Lederbogen, F., Ulshofer, E., Peifer, A., *et al.* (2018). No association between cardiometabolic risk and neural reactivity to acute psychosocial stress. *Neuroimage Clinical*, **20**, 1115–22. doi: 10.1016/j.nicl.2018.10.018.

Maldjian, J.A., Laurienti, P.J., Kraft, R.A., Burdette, J.H. (2003). An automated method for neuroanatomic and cytoarchitectonic atlas-based interrogation of fMRI data sets. *NeuroImage*, **19**, 1233–9.

Morey, R.D., Rouder, J.N. (2011). Bayes factor approaches for testing interval null hypotheses. *Psychological Methods*, **16**(4), 406–19. doi: 10.1037/a0024377.

Muscatell, K.A., Eisenberger, N.I. (2012). A social neuroscience perspective on stress and health. *Social and Personality Psychology Compass*, **6**, 890–904. doi: 10.1111/j.1751-9004.2012.00467.x.

Nord, C.L., Gray, A., Charpentier, C.J., Robinson, O.J., Roiser, J.P. (2017). Unreliability of putative fMRI biomarkers during emotional face processing. *NeuroImage*, **156**, 119–27. doi: 10.1016/j.neuroimage.2017.05.024.

Oppenheimer, S.M., Cechetto, D.F. (2016). Insular cortex and the regulation of cardiac function. *Comphrehensive Physiology*, **6**, 1081–133.

Osborne, M.T., Ishai, A., Hammad, B., *et al.* (2019). Amygdalar activity predicts future incident diabetes independently of adiposity. *Psychoneuroendocrinology*, **100**, 32–40. doi: 10.1016/j.psyneuen.2018.09.024.

Oygarden, H. (2017). Carotid intima-media thickness and prediction of cardiovascular disease. *Journal of the American Heart Association*, **6**(1). doi: 10.1161/JAHA.116.005313.

Peters, S.A., den Ruijter, H.M., Bots, M.L., Moons, K.G. (2012). Improvements in risk stratification for the occurrence of cardiovascular disease by imaging subclinical atherosclerosis: a systematic review. *Heart*, **98**(3), 177–84. doi: 10.1136/heartjnl-2011-300747.

Pignoli, P., Tremoli, E., Poli, A., Oreste, P., Paoletti, R. (1986). Intimal plus medial thickness of the arterial wall: a direct measurement with ultrasound imaging. *Circulation*, **74**(6), 1399–406.

Plichta, M.M., Grimm, O., Morgen, K., *et al.* (2014). Amygdala habituation: a reliable fMRI phenotype. *NeuroImage*, **103**, 383–90. doi: 10.1016/j.neuroimage.2014.09.059.

Polak, J.F., Szklo, M., O'Leary, D.H. (2017). Carotid intima-media thickness score, positive coronary artery calcium score, and incident coronary heart disease: the multi-ethnic study of atherosclerosis. *Journal of the American Heart Association*, **6**(1). doi: 10.1161/JAHA.116.004612.

Poldrack, R.A., Huckins, G., Varoquaux, G. (2019). Establishment of best practices for evidence for prediction: a review. *JAMA Psychiatry*. doi: 10.1001/jamapsychiatry.2019.3671.

R-Core-Team. (2014). *R: A Language and Environment for Statistical Computing*, R Foundation for Statistical Computing: Vienna, Austria. Retrieved from: http://www.R-project.org/

Rozanski, A., Blumenthal, J.A., Kaplan, J. (1999). Impact of psychological factors on the pathogenesis of cardiovascular disease and implications for therapy. *Circulation*, **99**(16), 2192–217.

Ruiz Vargas, E., Sörös, P., Shoemaker, J.K., Hachinski, V. (2016). Human cerebral circuitry related to cardiac control: a neuroimaging meta-analysis. *Annals of Neurology*, **79**, 709–16.

Scheinost, D., Noble, S., Horien, C., *et al.* (2019). Ten simple rules for predictive modeling of individual differences in neuroimaging. *NeuroImage*, **193**, 35–45. doi: 10.1016/j.neuroimage.2019.02.057.

Sojkova, J., Najjar, S.S., Beason-Held, L.L., *et al.* (2010). Intima-media thickness and regional cerebral blood flow in older adults. *Stroke*, **41**(2), 273–9. doi: 10.1161/STROKEAHA.109.566810.

Stein, J.H., Korcarz, C.E., Hurst, R.T., *et al.* (2008). Use of carotid ultrasound to identify subclinical vascular disease and evaluate cardiovascular disease risk: a consensus statement from the American Society of Echocardiography carotid intima-media thickness task force endorsed by the Society for Vascular Medicine. *Journal of the American Society of Echocardiography*, **21**, 93–108.

Suls, J., Bunde, J. (2005). Anger, anxiety, and depression as risk factors for cardiovascular disease: the problems and implications of overlapping affective dispositions. *Psychological Bulletin*, **131**(2), 260–300.

Tawakol, A., Ishai, A., Takx, R.A., *et al.* (2017). Relation between resting amygdalar activity and cardiovascular events: a longitudinal and cohort study. *Lancet*, **389**, 834–45. doi: 10.1016/S0140-6736(16)31714-7.

Thayer, J.F., Ahs, F., Fredrikson, M., Sollers, J.J., 3rd, Wager, T.D. (2012). A meta-analysis of heart rate variability and neuroimaging studies: implications for heart rate variability as a marker of stress and health. *Neuroscience and Biobehavioral Reviews*, **36**(2), 747–56. doi: 10.1016/j.neubiorev.2011.11.009.

Tibshirani, R. (1996). Regression shrinkage and selection via the lasso. *The Journal of Royal Statistical Society, Series B Statistical Methodology*, **58**, 267–88.

Tottenham, N. (2006). *MacBrain Face Stimulus Set*. Retrieved from: http://www.macbrain.org/resources.htm.

Tzourio-Mazoyer, N., Land.0.eau, B., Papathanassiou, D., *et al.* (2002). Automated anatomical labeling of activations in SPM using a macroscopic anatomical parcellation of the MNI MRI single-subject brain. *NeuroImage*, **15**, 273–89.

Wager, T.D., Atlas, L.Y., Leotti, L.A., Rilling, J.K. (2011). Predicting individual differences in placebo analgesia: contributions of brain activity during anticipation and pain experience. *The Journal of Neuroscience*, **31**(2), 439–52. doi: 10.1523/JNEUROSCI.3420-10.2011.

Wager, T.D., Atlas, L.Y., Lindquist, M.A., Roy, M., Woo, C.W., Kross, E. (2013). An fMRI-based neurologic signature of physical pain. *The New England Journal of Medicine*, **368**(15), 1388–97. doi: 10.1056/NEJMoa1204471.

Wendell, C.R., Waldstein, S.R., Evans, M.K., Zonderman, A.B. (2017). Distributions of subclinical cardiovascular disease in a socioeconomically and racially diverse sample. *Stroke*, **48**(4), 850–6. doi: 10.1161/STROKEAHA.116.015267.

Wong, M., Edelstein, J., Wollman, J., Bond, M.G. (1993). Ultrasonic-pathological comparison of the human arterial wall. Verification of intima-media thickness. *Arteriosclerosis and Thrombosis*, **13**(4), 482–6.

Woo, C.W., Wager, T.D. (2016). What reliability can and cannot tell us about pain report and pain neuroimaging. *Pain*, **157**(3), 511–3. doi: 10.1097/j.pain.0000000000000442.

Woo, C.W., Chang, L.J., Lindquist, M.A., Wager, T.D. (2017). Building better biomarkers: brain models in translational neuroimaging. *Nature Neuroscience*, **20**(3), 365–77. doi: 10.1038/nn.4478.

Zhao, P., Rocha, G., & Yu, B. (2009). The composite absolute penalties family for grouped and hierarchical variable selection. *Annals of Statistics*, **37**, 3468–3497.